II. 臨床研究

治療　外科治療

広汎前立腺切除術

Extended radical prostatectomy

藤元博行

Key words：局所進行前立腺癌，手術療法，ホルモン療法

はじめに

著者らは，局所の切除をより完全に行うことで局所進行前立腺癌に対して根治の可能性を追求してきた．いろいろな手技の改良を経て前立腺周囲を広汎に切除する広汎前立腺切除術を確立し，現在でも更なる改良への努力を続けている．これまでの経過なども含め，この手技について概説する．

1. 併用内分泌療法に関する変遷

広汎前立腺切除術の開発により，2000年からは術後の即時ホルモン療法は施行しない方針とした．それは，即時ホルモン療法を施行するとPSA failureの解釈を曖昧にし，手術の効果が確認できないからである．一方この時期，術前ホルモン療法(NHT)は継続された．NHTのRCTの結果[1-3]からdownstagingは期待できず，NHTの効果を期待して縮小手術を行うのは危険である．しかし，NHTを施行することにより前立腺体積が減少することは明らかである．確実な切除断端を確保することは治療成績の向上につながることも明らかである．したがって，NHTは主にdownsizingを目的とした．特に近年ではPSAにより発見される前立腺癌が増えており，このような病態では前立腺尖部腹側に病巣が多く存在することが認識されている[4]．前立腺尖部と恥骨との間が拡大することにより少しでも距離が確保されることは切除に際して有利に働くはずと考えた．以上のコンセプトに基づき，cT3前立腺癌に対してはNHT併用手術療法の治療を行った．

その結果，良好な病理結果が必ずしも，術後の成績に反映しない事態も発生した．このため2006年からはホルモン療法を一切施行せず，切除を行うことで治療効果を確認するに至っている．

2. 広汎前立腺切除術：その手術方法

a. 直腸固有筋膜の処理と尖部の確認

広汎前立腺切除術については既に幾つかの成書に記載してきた[5,6]．誌面の関係でこの手術のポイントのみを解説する．

まず，内骨盤筋膜を切開して直腸固有筋層が認められるまで肛門挙筋を剥離し，固有筋膜を縦切開し直腸筋層を確認する．剥離を進めるとあるポイントから剥離ができなくなる．これは腱中心に到達したことを意味する．直腸を外側に牽引しながら前立腺後面との間の剥離を進める．直腸尿道筋は精嚢付近で前立腺に付着しており，この部位では電気メスで切開することで初めて剥離が可能となる．最後に中枢で直腸筋層の露出を横方向に進める．これは前立腺を逆行性に処理する際，直腸尿道筋，直腸筋層，前

Hiroyuki Fujimoto: Urology Division, National Cancer Center Hospital　国立がんセンター中央病院 泌尿器科

0047-1852/07/¥40/頁/JCLS

立腺を剥離する際の重要なメルクマールとなる.

b. 前立腺尖部の把握とDVCの処理

PSA eraの現在，前立腺尖部前面が癌の好発部位であり，尖部をいかに的確に把握するかが，確実な切除断端の確保のみならず尿道機能の確保，勃起神経温存において重要である.

先に剥離した直腸筋層と前立腺の間にクーパーを挿入し前立腺尿道移行部後面を認識する. 尿道外側に付着する肛門挙筋を最小限剥離し，尿道後面とおぼしき部位で，尿道外周に沿うようにメッチェンバウムを滑り込ませ，lateral pelvic fasciaを1枚貫通させることで尿道後面に到達できる. 尿道後面に鉗子を通し，血管テープで尿道後面を把持する.

DVCの処理ではbunching処理は2針程度運針する. これは必要以上に運針を行うと，前立腺被膜が変形し，前立腺尖部の把握が不正確になることを嫌っているためである. 前立腺を牽引してDVCの最も末梢側にstay sutureをおき，出血に際して順次，収束結紮を繰り返し，止血する.

前立腺尖部の位置関係を触診・視診あるいは前立腺を可動させて最終確認を行った後，DVCを切開する. 前立腺被膜と収束結紮されたDVCの深さに注意しながら処理を進める. DVCの切開では鋭的な切断に変更している. これは尿道筋層，あるいはその中に進展しているかもしれない前立腺組織の認識をより確実にするためである. 電気メスを使用すると全体が熱変性を受けることで確認しにくい. 外側では前立腺被膜が12時の位置より更に末梢に進展していることがある. 外尿道括約筋を確認した後は，外側の被膜と切開している尿道筋層との間に，括約筋でもなく，被膜でもない組織が存在していないことを確認しながら処理を進める. このような処理を行うと通常は尿道がU時に処理される. 12時の位置で切開を進め尿道カテーテルを確認する. その後，尿道に吻合糸をかける.

c. 膀胱頸部の処理

本法ではいわゆるposterior peel法は全く行わない. 精嚢と膀胱三角部後面の剥離を行った後，尿道カテーテルのバルーンを膀胱前面で触知する. 明らかに前立腺が存在しないと認識できる場所から膀胱前面を横方向に切開し，尿道カテーテルを膀胱外に引き出し，尿管口ならびに三角部を確認して，原則三角部のみを残して膀胱頸部を離断する.

前立腺を摘出後，膀胱頸部を縫縮する. ポイントは2つである. 1つは筋層をしっかり縫合するとともに膀胱粘膜が反転しないようにする. これは膀胱頸部の接着に逆効果になるとの認識からである. 最終的に7-8針必要なことが多いが，順次，膀胱筋層を縫縮して内尿道口を形成する. 縦長で1.5-2cm程度の内尿道口を形成している. 広汎前立腺切除術では直腸筋層が露出されており，膀胱筋層との間で瘻孔を作る危険性がある. このため膀胱筋層の縫縮の後，露出された膀胱筋層の外側の膀胱漿膜と脂肪織を縫縮し2層に縫縮するようにしている. その後，尿道と吻合する.

3. NHT併用広汎前立腺切除術の結果

a. cT3aに対する切除法とPSA非再発率

NHT併用広汎前立腺切除術と通常の切除法のPSA再発(0.2ng/ml以上と定義)をGleason score，PSA値との関係で示したのが**図1**である. 通常切除術200例，ならびに広汎前立腺切除術135例の背景を**表1**に示した. このデータから概要がうかがえるが，広汎前立腺切除術ではPSA 20-40ng/mlくらいまでをカバーしているようにみえる.

b. 結　果

NHT併用広汎前立腺切除術を施行された393全症例(PSA: 2.45-124.7ng/ml(平均15.8，中央値10.7)，年齢：49-77歳(平均65.0，中央値65.0)，Gleason score: 5-10(平均7.3，中央値7)，観察期間：4-78カ月(平均27.0，中央値24.6))におけるPSA非再発率を解析した. T stage，PSA，Gleason score，切除断端，精嚢浸潤，リンパ節転移をパラメーターとしてハザードモデルで検討した結果，再発の危険因子は精嚢浸潤の有無($p<0.0001$)とPSA値($p=0.0001$)のみであった. 精嚢浸潤の有無別PSA非再発率を**図2**

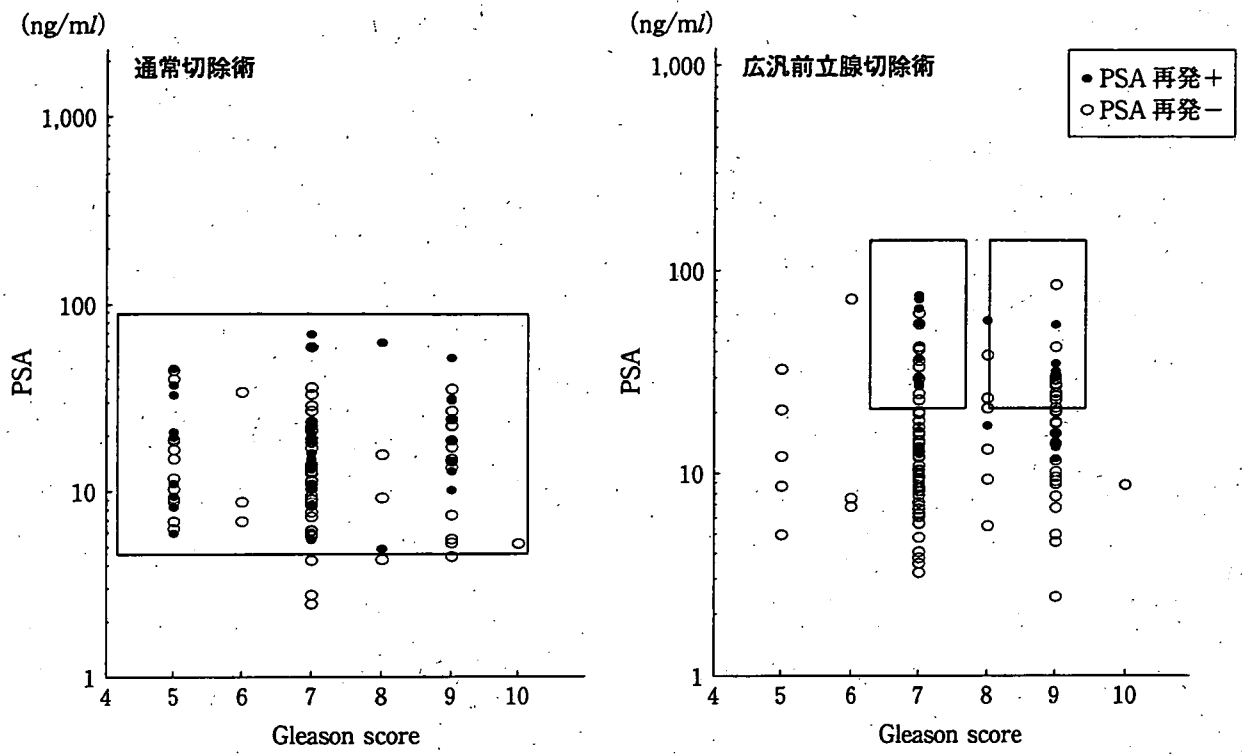

図1　cT3a に対して NHT を施行した PSA 再発

表1　cT3a NHT 症例の背景

手術法	症例数	年　齢（中央値）	PSA（中央値）	Gleason score	観察年（中央値）
通常切除術	200	65.8(66.0)	21.9(13.65) 2.4-232.6	7.0(5-10)	5.1(5.3)
広汎切除術	135	65.2(65.0)	19.25(13.24) 2.4-84.8	7.5(5-10)	2.2(2.0)

(左)に示した．pT4 前立腺癌の中には精嚢浸潤の有無にかかわらず pT4 と判定されるが，精嚢浸潤のない pT4 とある pT4 のデータも図2(右)に示した．

c. 結　論

結論は単純であり，精嚢浸潤のない局所前立腺癌では広汎前立腺切除術により5年非再発率は86.1%，精嚢浸潤があると33.5%と切除が不成功に終わるということであった．一方で断端の状況と治療成績が必ずしも相関していないようにも思われた．再発の原因は何か？ 病態が細胞レベルで転移している可能性と手術操作に起因したことの両方の可能性が考えられた．

おわりに

cT3 前立腺癌に対して，局所をより完全に切除することにより，治療成績の向上が期待できないかとの問題意識から広汎前立腺切除術を開発した．この手術法をもって cT3 前立腺癌に対して治療を行ったところ，この手術の限界は現在の方法では精嚢浸潤陽性である．

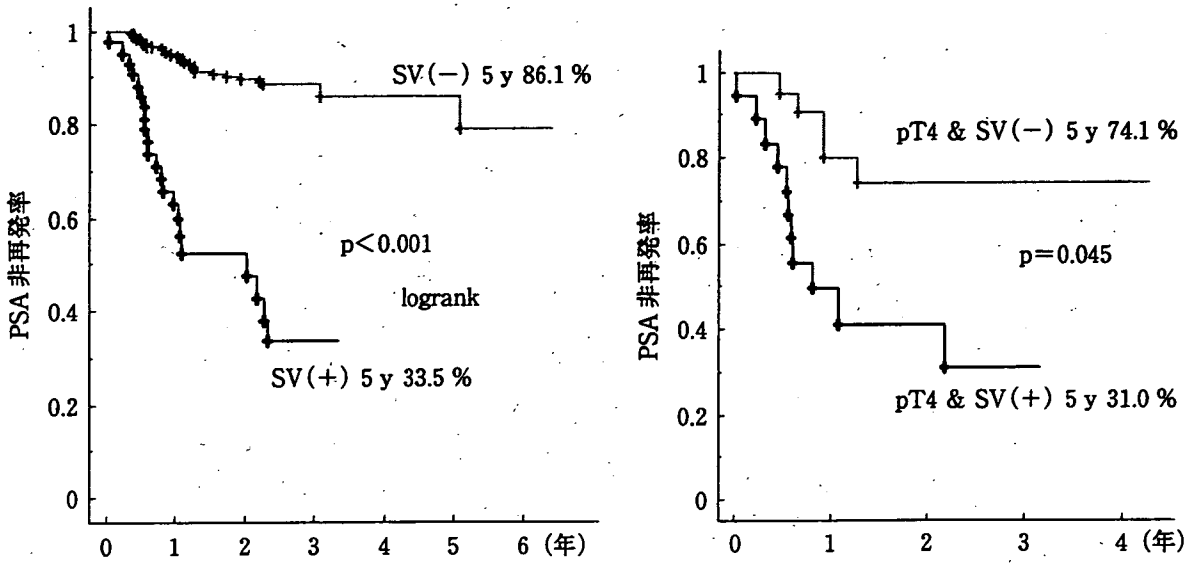

図2 PSA failure: 広汎前立腺切除術

■文 献

1) Klotz LH, et al: CUOG randomized trial of neoadjuvant androgen ablation before radical prostatectomy: 36-month post-treatment PSA results. Canadian Urologic Oncology Group. Urology **53** (4): 757-763, 1999.
2) Gleave ME, et al: Randomized comparative study of 3 versus 8-month neoadjuvant hormonal therapy before radical prostatectomy: biochemical and pathological effects. J Urol **166**(2): 500-506, 2001.
3) Aus G, et al: Three-month neoadjuvant hormonal therapy before radical prostatectomy: a 7-year follow-up of a randomized controlled trial. BJU Int **90**: 561-566, 2002.
4) Takashima R, et al: Anterior distribution of Stage T1c nonpalpable tumors in radical prostatectomy specimens. Urology **59**: 692-697, 2002.
5) 中川 徹ほか：前立腺全摘除術．新 癌の外科—手術手技シリーズ2 泌尿器癌(垣添忠生監，藤元博行編)，p89-107，メジカルビュー社，2001.
6) 藤元博行：非神経温存前立腺広汎切除術における排尿機能．Urology View **5**(2): 51-57, 2007.

Original Report

Ukihide Tateishi[1]
Tadashi Hasegawa[2]
Hiroaki Onaya[1]
Mitsuo Satake[1]
Yasuaki Arai[1]
Noriyuki Moriyama[1]

Myxoinflammatory Fibroblastic Sarcoma: MR Appearance and Pathologic Correlation

OBJECTIVE. The purpose of our study was to define the MR appearance of myxoinflammatory fibroblastic sarcoma of the soft tissues and to make correlations with the histopathologic features.

CONCLUSION. Myxoinflammatory fibroblastic sarcoma is an uncommon malignancy that typically affects adult subjects, who present with painless swelling. This lesion manifests on MR images as a poorly circumscribed mass involving the underlying tendon sheath in the distal extremities.

Received June 2, 2004; accepted after revision July 28, 2004.

Supported in part by grant for Scientific Research Expenses for Health and Welfare Programs, The Foundation for the Promotion of Cancer Research, and second-term Comprehensive 10-year Strategy for Cancer Control.

[1]Division of Diagnostic Radiology, National Cancer Center Hospital and Institute, Tsukiji, Chuo-Ku, 104-0045, Tokyo, Japan. Address correspondence to U. Tateishi.

[2]Pathology Division, National Cancer Center Hospital and Institute, Tsukiji, Tokyo, Japan.

AJR 2005;184:1749–1753

0361–803X/05/1846–1749

Myxoinflammatory fibroblastic sarcoma of the soft tissues is a rare low-grade tumor of uncertain origin that usually arises in the hands and feet. Myxoinflammatory fibroblastic sarcoma was first described in 1998 by Meis-Kindblom and Kindblom [1]. Montgomery et al. [2] named the tumor "inflammatory myxohyaline tumor" of the distal extremities with virocyte or Reed-Sternberg-like cells. Histologic characteristics are the spindle to epithelioid neoplastic cells as the manifestation of malignancy admixed with the myxoid and hyalinized matrix, the inflammatory infiltrate, and bizarre virocyte or Reed-Sternberg-like cells with enlarged vesicular nuclei [1–3].

More than 100 cases of myxoinflammatory fibroblastic sarcoma have been reported, with a large series identified in two articles [1–6]. However, MRI findings of myxoinflammatory fibroblastic sarcoma have rarely been documented. The purpose of this study was to characterize the MR appearance of myxoinflammatory fibroblastic sarcoma and to correlate that appearance with the histopathologic features.

Materials and Methods

MR images of all patients with pathologically proven myxoinflammatory fibroblastic sarcoma at our institution were retrospectively reviewed. Our institutional review board gave its approval for a review of patient records and images. The patients were identified by review of our institution's pathology database for a 2-year period. The affected patients included three males and one female who ranged in age from 15 to 62 years old (mean age, 35 years). All histopathologic specimens were reviewed by an experienced pathologist to confirm the diagnosis. Histopathologic examination in all patients showed spindle and epithelioid tumor cells with mild nuclear atypia. Ganglionlike cells and Reed-Sternberg-like cells were also prominent in all cases. Inflammatory cells, including neutrophils, lymphocytes, and eosinophils, were densely present in all cases. Immunohistochemistry was performed in all patients, and all tumors displayed immunoreactivity to vimentin, smooth-muscle actin, and CD34. These histopathologic characteristics were compatible with the diagnosis of myxoinflammatory fibroblastic sarcoma [7]. Medical records were reviewed by one of the authors for presenting complaints, disease progression, and outcome. Radiographs, available for all patients, were also evaluated by two radiologists for the presence of soft-tissue masses or nodules, mineralization, and bone destruction. The findings were recorded by consensus.

T1- and T2-weighted MR images were obtained in the sagittal and coronal planes using a surface coil. T1-weighted conventional spin-echo MR images were obtained using a 20-cm field of view, 3.5- to 5-mm section thickness, TR range/TE of 450–520/15, 160 × 256 matrix, and 2 signals acquired. T2-weighted fast spin-echo acquisitions with ($n = 3$) or without ($n = 1$) fat suppression were performed using a 20-cm field of view, 3.5- to 5-mm section thickness, 3,600–4,000/120, 160 × 256 ma-

trix, and 2 signals acquired. After the IV administration of 0.1 mmol of gadopentetate dimeglumine (Magnevist, Schering) per kilogram of body weight, transverse T1-weighted images with (n = 3) or without (n = 1) fat suppression were obtained in the sagittal and coronal planes.

MR images were reviewed by two radiologists and findings were recorded by consensus. Images were evaluated for lesion location and size, depth (superficial or deep), shape of margin (well or ill defined), and the presence or absence of extracompartmental extension. To define depth, superficial lesions did not involve the superficial fascia, and deep lesions were deep in relation to or invaded the superficial fascia. The relationship between tumor and the underlying tendon sheath was also evaluated. MR images were evaluated for predominant signal intensity characteristics (low, intermediate, high), signal homogeneity or heterogeneity, and enhancement characteristics. On T1-weighted images, low signal intensity was defined as signal intensity less than that of muscle; intermediate signal intensity, similar to that of muscle; and high signal intensity, similar to that of fat. On T2-weighted images, low signal intensity was defined as signal intensity similar to that of muscle; intermediate signal intensity, greater than that of muscle but less than that of fat; and high signal intensity, equal to or greater than that of fat. Tumor enhancement was visually graded as greater than, less than, or equal to that of surrounding muscle and vessels.

Results

Clinical Features

All patients were symptomatic at presentation. Presenting complaints were painless swelling of the distal extremities. The mean symptom duration was 4.8 months. Tumors arose from the feet (n = 2), hands (n = 1), and fingers (n = 1). All patients received excisional biopsy for definitive diagnosis and primary therapy. Surgical margins were adequate in three patients and inadequate in one patient. The one patient with an inadequate surgical margin underwent subsequent wide resection. Chemotherapy and radiation therapy were not included in the treatment regimen in any patient. Local recurrence occurred 26.5 months after the initial surgery in two patients. These patients received wide resection. At the latest follow-up (27–82 months; mean, 45 months), no patients had developed further recurrence or metastasis.

MRI Findings and Pathologic Correlations

The gross characteristics of the resected specimens featured multinodular architecture corresponding to MRI features. The mean tumor diameter was 2.4 cm (range, 1.2–3.0 cm). Tumors were located along the tendon sheath in all patients. Findings of extensive involvement surrounding the tendon sheath by the tumor were seen. In two patients, the tumor existed beneath the tendon sheath (Fig. 1), and in two it involved the surrounding tendon sheath diffusely and focally infiltrated the dermis (Fig. 2). One patient had an ill-defined, irregularly marginated mass involving the ulnar nerve and the tendon sheath of the flexor carpi ulnaris (Fig. 2).

Cortical invasion was not identified in any patient on radiographs. All tumors showed predominantly low signal intensity relative to muscle on T1-weighted MR images (Fig. 3). Two lesions showed moderate and homogeneous enhancement after the IV administration of contrast material (Figs. 1 and 3). The cut surface of resected specimens showed solid nests of neoplastic cells that featured spindle and epithelioid cells with higher cellularity, which corresponded to homogeneous enhancement on contrast-enhanced MR images. Two lesions showed heterogeneous enhancement of the tumor that correlated with geographic areas of the myxoid stromal matrix on microscopic observations (Fig. 4). On T2-weighted MR images, all lesions had intermediate signal intensity greater than that of muscle but less than that of fat (Fig. 2). In all cases, the cut surface of specimens revealed solid nests of cellular areas with foci of hyalinized collagen fibers and hypocellular areas with a myxoid stromal

A

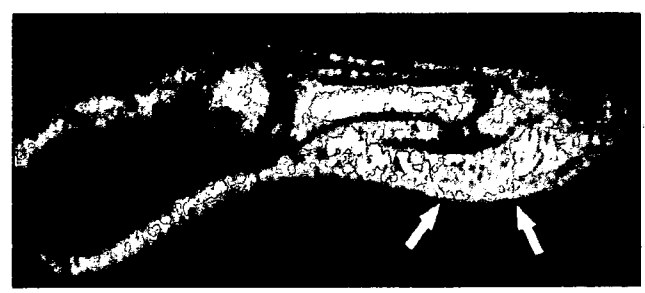

B

C

Fig. 1.—Myxoinflammatory fibroblastic sarcoma in 62-year-old man with painless mass in finger.
A, Sagittal T1-weighted MR image (TR/TE, 450/15) shows poorly circumscribed mass beneath tendon sheath of flexor hallucis longus (*arrows*).
B, Sagittal contrast-enhanced T1-weighted MR image (450/15) shows homogeneous enhancement (*arrows*).
C, Photograph of histopathologic specimen shows solid nests of spindle and epithelioid tumor cells with foci of inflammatory cell infiltrate (*arrows*).

matrix, which corresponded to the imaging appearance of intermediate signal intensity on T2-weighted MR images.

Two patients developed recurrent tumors and underwent follow-up MRI after treatment. One patient developed a mass of sheetlike appearance beneath the dorsal portion of the underlying tendon sheath (Fig. 3). Signal characteristics and homogeneous enhancement patterns were similar to those of the primary tumors. Histopathologic examination of this patient showed an infiltrate of lymphoid cells and a marked proliferation of spindle-shaped tumor cells surrounding the tendon sheaths.

In the second patient, a mass of branching pattern occurred along the extensor digitorum longus tendon sheaths of the second and fourth toes without distortion of the architecture of the tendon sheaths (Fig. 4). This patient had also MRI findings suggesting capsular involvement in the metatarsophalangeal joint of the second toe. Histopathologic examination revealed that the tumor arose from the extensor digitorum longus tendon sheaths and also involved the extensor digitorum brevis tendon sheath, cutaneous nerve, and dermis.

Discussion

Myxoinflammatory fibroblastic sarcoma is a rare tumor of the subcutaneous soft tissue that can arise on the trunk but most commonly occurs in the distant extremities [1, 2]. According to the literature and our experience, myxoinflammatory fibroblastic sarcoma is a tumor that most commonly affects adults who are symptomatic at presentation [1, 2]. All patients in our series were symptomatic, with common complaints of a painless mass.

Myxoinflammatory fibroblastic sarcoma has a relatively good prognosis with a long life expectancy despite frequent local recurrence [1–3]. Two of our patients developed local recurrence, with an average duration of 26.5 months. According to the literature, the local recurrence rate in patients with myxoinflammatory fibroblastic sarcoma ranges from 22% to 67% [1, 2]. The metastasis rate in patients with myxoinflammatory fibroblastic sarcoma is uncertain. Metastases have been reported to develop in only a few cases [1].

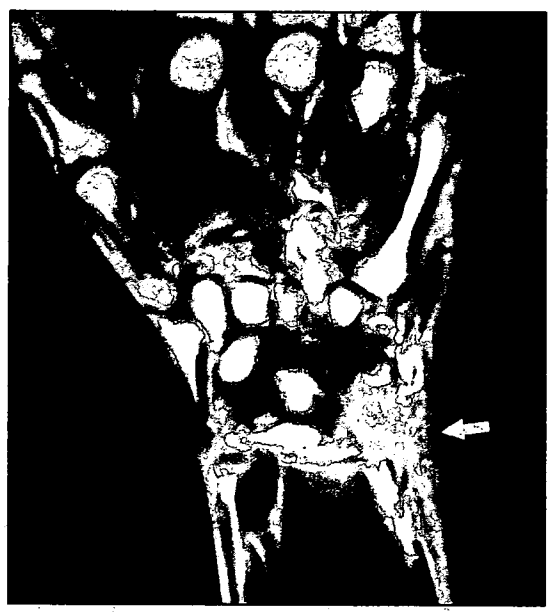

A

B

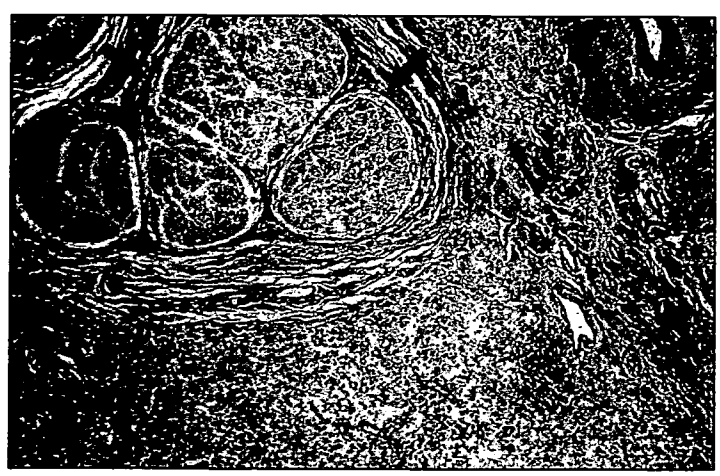

C

Fig. 2.—Myxoinflammatory fibroblastic sarcoma in 31-year-old man with painless mass in subcutaneous soft tissue of wrist.
A, Coronal contrast-enhanced T1-weighted MR image (TR/TE, 520/15) shows poorly circumscribed mass with ill-defined border. Tumor involves surrounding tendon sheath diffusely and focally infiltrates dermis (*arrow*).
B, Axial contrast-enhanced T1-weighted MR image (520/15) shows mass involving ulnar nerve (*arrow*) and tendon sheath of flexor carpi ulnaris (*arrowhead*).
C, Photograph of histopathologic specimen reveals that numerous small nodules consisting of tumor cells infiltrate along ulnar nerve (*arrows*).

In all of our patients, excisional biopsy for definitive diagnosis and primary therapy was performed. However, tumor margins in one of our patients were inadequate and the patient underwent subsequent wide resection. Tumors are often removed piecemeal by surgical procedures, with curative wide resection considered to be the adequate treatment of choice [1].

Grossly, myxoinflammatory fibroblastic sarcoma forms a poorly circumscribed mass surrounding the tendon sheath that may extend into the dermis and skeletal muscle. Microscopically, the tumor is characterized by solid nests of atypical spindle and epithelioid cells in a myxoid stroma and dense inflammatory infiltrates. The tumor cells often have large vesicular nuclei similar to those of virocytes or Reed-Sternberg cells. The immunophenotype is positive for vimentin, with variable immunoreactivity for CD34, CD68, cytokeratin, and smooth-muscle actin [1–6].

On MR images, myxoinflammatory fibroblastic sarcoma typically manifests as a poorly circumscribed mass with a multinodular appearance. Extensive involvement surrounding the tendon sheath is also a common feature.

The appearance of the extension along the tendon sheath in this tumor is similar to that seen in tenosynovitis. Differentiating tenosynovitis from myxoinflammatory fibroblastic sarcoma solely on MRI findings is difficult. Tenosynovitis also can lead to an ill-defined soft-tissue mass or enlargement of its sheath. However, this condition typically manifests as the accumulation of fluid with increased signal intensity of the affected tendon on T2-weighted MR images [8]. Clinical characteristics can allow the differentiation of tenosynovitis from myxoinflammatory fibroblastic sarcoma because tenosynovitis often decreases in size during the course of disease, whereas myxoinflammatory fibroblastic sarcoma usually grows with infiltration [1].

MRI findings of myxoinflammatory fibroblastic sarcoma also closely resemble those of giant cell tumors of the tendon sheath, proliferative fasciitis, acral fibromyxoma, myxoid

A

B

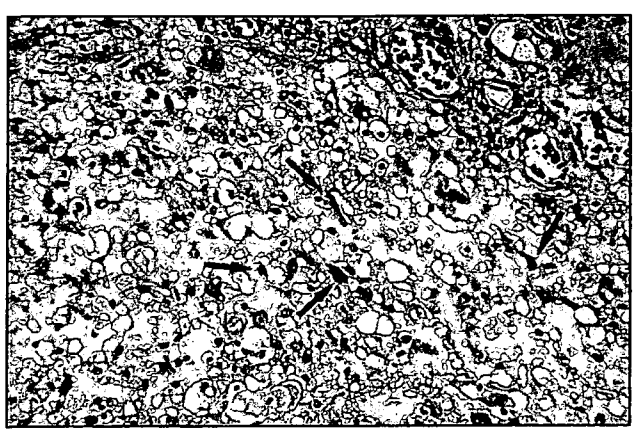

C

Fig. 3.—Myxoinflammatory fibroblastic sarcoma in foot of 32-year-old woman with local recurrence.

A, Sagittal T2-weighted MR image (TR/TE, 3,600/120) shows mass of sheetlike appearance beneath dorsal portion of tendon sheath. Tumor shows intermediate signal intensity, greater than that of muscle (*arrow*).

B, Sagittal contrast-enhanced fat-saturated T1-weighted MR image (520/15) shows homogeneous enhancement of tumor (*arrows*).

C, Photograph of histopathologic specimen shows sheetlike proliferation of spindle-shaped tumor cells (*arrows*) with ganglionlike cells, Reed-Sternberg-like cells, and lymphoid cells surrounding tendon sheaths.

A

B

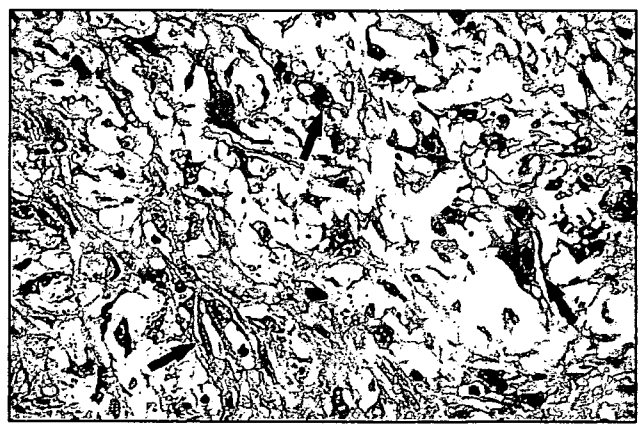

C

Fig. 4.—Myxoinflammatory fibroblastic sarcoma in foot of 24-year-old man with local recurrence.
A, Coronal fat-saturated T2-weighted MR image (TR/TE, 3,500/105) shows mass of branching pattern that occurred along extensor digitorum longus tendon sheaths of second and fourth toes (*arrows*). Tumor shows intermediate signal intensity, greater than that of muscle.
B, Coronal contrast-enhanced T1-weighted MR image (520/15) shows heterogeneous enhancement of tumor (*arrows*).
C, Photograph of histopathologic specimens shows proliferation of spindle-shaped tumor cells (*arrows*) with prominent nucleoli in abundant myxoid stromal matrix.

liposarcoma, and myxofibrosarcoma [9–13]. These conditions could not be distinguished radiologically from myxoinflammatory fibroblastic sarcoma on the basis of our study results. Signal characteristics and enhancement patterns were nonspecific. However, heterogeneous enhancement on contrast-enhanced MR images corresponded to geographic areas of the myxoid stromal matrix in the pathologic specimens. In two of our patients, MRI findings of recurrent tumors were ill defined and the tumors had sheetlike appearances involving the tendon sheath. A significant association may exist between recurrent tumors and the tendon sheath.

In summary, myxoinflammatory fibroblastic sarcoma typically affects adult subjects as a painless mass of the distal extremities at presentation. Myxoinflammatory fibroblastic sarcoma usually manifests on MR images as a multinodular and poorly circumscribed mass involving the surrounding tendon sheath. Although it is unlikely that such a rare condition could reasonably be diagnosed on the basis of MRI findings alone, the condition should be considered in the differential diagnosis of a soft-tissue mass in the distal extremities of adult patients.

References

1. Meis-Kindblom JM, Kindblom LG. Acral myxoinflammatory fibroblastic sarcoma: a low-grade tumor of the hands and feet. *Am J Surg Pathol* 1998:22:911–924
2. Montgomery EA, Devaney KO, Giordano TJ, Weiss SW. Inflammatory myxohyaline tumor of distal extremities with virocyte or Reed-Sternberg-like cells: a distinctive lesion with features simulating inflammatory conditions, Hodgkin's disease, and various sarcomas. *Mod Pathol* 1998:11:384–391
3. Lambert I, Debiec-Rychter M, Guelinckx P, Hagemeijer A, Sciot R. Acral myxoinflammatory fibroblastic sarcoma with unique clonal chromosomal changes. *Virchows Arch* 2001:438:509–512
4. Jurcic V, Zidar A, Montiel MD, et al. Myxoinflammatory fibroblastic sarcoma: a tumor not restricted to acral sites. *Ann Diagn Pathol* 2002:6:272–280
5. Sakaki M, Hirokawa M, Wakatsuki S, et al. Acral myxoinflammatory fibroblastic sarcoma: a report of five cases and review of the literature. *Virchows Arch* 2003:442:25–30
6. Pohar-Marinsek Z, Flezar M, Lamovec J. Acral myxoinflammatory fibroblastic sarcoma in FNAB samples: can we distinguish it from other myxoid lesions? *Cytopathology* 2003:14:73–78
7. Weiss SW, Goldblum JR. *Enzinger and Weiss's soft tissue tumors*, 4th ed. St. Louis, MO: Mosby, 2001:1552–1571
8. Mallefert JF, Dardel P, Cherasse A, Mistrih R, Krause D, Tavernier C. Magnetic resonance imaging in the assessment of synovial inflammation of the hindfoot in patients with rheumatoid arthritis and other polyarthritis. *Eur J Radiol* 2003:47:1–5
9. Llauger J, Palmer J, Monill JM, Franquet T, Bague S, Roson N. MR imaging of benign soft-tissue masses of the foot and ankle. *RadioGraphics* 1998:18:1481–1498
10. Kato K, Ehara S, Nishida J, Satoh T. Rapid involution of proliferative fasciitis. *Skeletal Radiol* 2004:33:300–302
11. Fetsch JF, Laskin WB, Miettinen M. Superficial acral fibromyxoma: a clinicopathologic and immunohistochemical analysis of 37 cases of a distinctive soft tissue tumor with a predilection for the fingers and toes. *Hum Pathol* 2001:32:704–714
12. Tateishi U, Hasegawa T, Beppu Y, Kawai A, Satake M, Moriyama N. Prognostic significance of MRI findings in patients with myxoid-round cell liposarcoma. *AJR* 2004:182:725–731
13. Munk PL, Sallomi DF, Janzen DL, et al. Malignant fibrous histiocytoma of soft tissue imaging with emphasis on MRI. *J Comput Assist Tomogr* 1998:22:819–826

World J. Surg. 29, 885–889 (2005)
DOI: 10.1007/s00268-005-7878-x

WORLD
Journal of
SURGERY

Arterial Reconstruction during Pancreatoduodenectomy in Patients with Celiac Axis Stenosis—Utility of Doppler Ultrasonography

Satoshi Nara, M.D.,[1] Yoshihiro Sakamoto, M.D.,[1] Kazuaki Shimada, M.D.,[1] Tsuyoshi Sano, M.D.,[1] Tomoo Kosuge, M.D.,[1] Yuh Takahashi, M.D.,[1] Hiroaki Onaya, M.D.,[2] Junji Yamamoto, M.D.[3]

[1]Hepatobiliary and Pancreatic Surgery Division, National Cancer Center Hospital, 5-1-1 Tsukiji, Chuo-ku, 104-0045, Tokyo, Japan
[2]Diagnostic Radiology Division, National Cancer Center Hospital, 5-1-1 Tsukiji, Chuo-ku, 104-0045, Tokyo, Japan
[3]Department of Gastrointestinal Surgery, Cancer Institute Hospital, 1-37-1 Kami-Ikebukuro, Toshima-ku, 170-8455, Tokyo, Japan

Published Online: June 16, 2005

Abstract. Celiac axis stenosis is found at an incidence of 2%–24% in the general population. During pancreatoduodenectomy in patients with celiac axis stenosis, division of the gastroduodenal artery from the common hepatic artery may cause acute ischemia of the upper abdominal organs, such as the liver, stomach, or spleen. Under these circumstances, the clinical indications of arterial reconstruction remain controversial. Between 1994 and 2003, seven patients with celiac axis stenosis (n = 4) or occlusion (n = 3) underwent pancreatoduodenectomy at our hospital. Arterial reconstruction, including division of the median arcuate ligament, was conducted in two patients; the replaced right hepatic artery was preserved in one patient, and no vascular refinement was undertaken in the remaining four of the seven patients. In two of the four patients without arterial reconstruction or preservation, the serum levels of liver enzymes were markedly elevated (> 800 IU/l) on postoperative day 1, and these patients subsequently developed liver abscesses. Two patients who underwent arterial reconstruction and three patients who showed no decrease in intrahepatic arterial flow under Doppler ultrasonography after clamping of the gastroduodenal artery developed no ischemic complications. Although our experience is limited, when intraoperative Doppler ultrasonography indicates a decrease in the hepatic arterial signals, we believe that reconstruction of the hepatic artery will be necessary to minimize ischemic complications in the liver in patients with celiac axis stenosis.

Celiac axis stenosis (CAS) is not a too rarely encountered condition. The reported incidence of CAS on angiographic examination is in the range of 12%–24% in European countries, and 2%–7% in Asian countries [1].

During pancreatoduodenectomy (PD) in patients with CAS, division of the gastroduodenal artery (GDA) from the common hepatic artery may cause abrupt ischemia of the upper abdominal organs, such as the liver, stomach, or spleen, especially if the collateral pathways from the superior mesenteric artery (SMA) are inadequate. To prevent ischemic complications in these organs, especially the liver, a variety of methods for arterial reconstruction [2–7] and preservation of the collateral pathways [8] have been reported. Some investigators argue, however, that the incidence of ischemic complications is low and that arterial reconstruction is seldom needed [9–11]. Thus, until now, the surgical indications for arterial reconstruction during PD for patients with CAS have not been established.

We review our experience of PD to assess the clinical indications for arterial reconstruction in patients with CAS, to avoid ischemic complications in the upper abdominal organs.

Patients and Methods

Patients and Diagnosis

Between 1994 and 2003, 357 patients underwent PD or pylorus-preserving PD (PPPD) at our hospital for the treatment of pancreatic cancer (n = 233), bile duct cancer (n = 55), duodenal cancer (n = 51), gallbladder cancer (n = 13), or other tumors of the pancreas head (n = 5). Whenever possible, the patients underwent preoperative angiography as part of the routine work-up. Among these, preoperative diagnosis of CA stenosis (n = 4) and occlusion (n = 3) was made in seven patients (2.0%). Celiac axis stenosis was suspected when the celiac tributaries were visualized through dilated collaterals on SMA angiography. The diagnosis of CAS was confirmed when the root of the celiac artery was stenotic on the angiographic images or in sagittal reformatted computed tomographic (CT) images. The diagnosis of celiac axis obstruction was confirmed when the root of CA could not be catheterized.

Treatments

Two patients underwent arterial revascularization. In one patient, division of the median arcuate ligament (MAL) was carried out (case 1, Table 1). The other patient in whom marked decrease of the intrahepatic arterial flow was visualized on Doppler ultrasonography (US) after the division of GDA, anastomosis between the middle colic artery (MCA) and the right gastroepiploic artery (RGEA) was performed (case 2). In another patient, the replaced right hepatic artery was preserved to maintain arterial flow into

Correspondence to: Yoshihiro Sakamoto, M.D., e-mail: yosakamo@ncc.go.jp

Table 1.

Case no.	Patient	Disease	CA status	Etiology	Adopted procedure	Doppler Us		GOT/GPT (1POD) (IU/l)	Ischemic complications	Discharge (POD)
						GDA clamp	After reconstruction			
1	65M	Ph Ca	Stenosis	MAL compression	Cutting of MAL	↓	↑	119/117	None	31
2	57M	Duo Ca	Occlusion	Atherosclerosis	MCA–RGEA anastomosis	↓	↑	1166/1221	None	35
3	61F	Duo Ca	Occlusion	Atherosclerosis	Preservation of replaced RHA	↑	—	73/87	None	128
4	64F	Ph Ca	Stenosis	Unknown	None	↑	—	118/95	None	31
5	86M	Ph Ca	Stenosis	Unknown	None	↑	—	121/131	None	52
6	48M	Ph Ca	Occlusion	CHA injury during angiography	None	↓	—	1396/1261	Liver abscess (POD 30)	60
7	55M	Ph Ca	Stenosis	Unknown	None	Not done	—	867/1019	Liver abscess (POD 52)	126

CA: celiac axis; GOT: glutamic oxaloacetic transaminase; GPT: glumatic pyruvic transaminase; Ph Ca: pancreatic head cancer; Duo Ca: duodenal cancer; MAL: median arcuate ligament; MCA: middle colic artery; RGEA: right gastroepiploic artery; CHA: common hepatic artery; RHA: right hepatic artery; POD: postoperative day; ↓: decrease of the intrahepatoc arterial flow; →: no remarkable change; ↑: increase of the intrahepatic arterial flow; US: ultrasound

the liver (case 3). The remaining four patients did not undergo any arterial reconstruction or preservation, based on the respective surgeons judgment.

Results

There was no postoperative mortality. In two out of the four patients (Cases 6 and 7) who did not undergo arterial reconstruction or preservation, the serum levels of the hepatic transaminases became markedly elevated (> 800 IU/L) on postoperative day 1, and these patients subsequently developed liver abscesses on postoperative days 30 and 52, respectively. The two patients (cases 1 and 2) who underwent arterial reconstruction and three patients (cases 3–5) who showed no decrease of intrahepatic arterial flow in on Doppler US after clamping of the GDA did not develop any ischemic complications. One patient (case 3) in whom the replaced right hepatic artery was preserved developed leakage of the pancreatojejunostomy, which was not attributed to ischemia (Table 1).

Case 1

A 65-year-old man presented with obstructive jaundice. Contrast-enhanced abdominal CT revealed a low-attenuation mass, 20 × 15 mm in size, located in the pancreatic head. On SMA angiography, the hepatic and splenic arteries were visualized serially via the GDA (Fig. 1A). Severe stenosis of the celiac artery at its root was demonstrated on sagittal reformatted CT imaging (Fig. 1B), and the CT image showed that some fibrous tissue connecting with bilateral curs covered the supraceliac aorta. Thus, a diagnosis of pancreatic cancer with CAS caused by compression of the MAL was made. The proposed operation was PPPD with possible arterial reconstruction.

After occlusion of the GDA, intraoperative Doppler US revealed an apparent decrease in the intrahepatic arterial flow (Fig. 2B), and thick fibrous tissue (MAL) was found to be masking the CA (Fig. 2A). The MAL was divided longitudinally and the root of the CA was fully exposed (Fig. 3 A). After division of the MAL, a marked increase in the intrahepatic arterial signals was observed, even with clamping of the GDA (Fig. 3B). Thereafter, the GDA was ligated and divided and PPPD was performed in the usual manner. The patient's postoperative course was uneventful and he was discharged on postoperative day 31.

Discussion

The surgical indications for hepatic arterial reconstruction during PD in patients with CAS remain unclear. Two of the four patients (50%) in our experience who did not undergo arterial reconstruction or preservation developed liver abscesses, whereas none of the three who underwent arterial reconstruction or preservation developed any ischemic complications. Even though our experience is limited, these results indicate that some form of arterial reconstruction may be necessary to avoid or minimize ischemic complications, when intraoperative Doppler US reveals a decrease in intrahepatic arterial signals. The preservation of collateral pathways from SMA to CA tributaries may be preferred, provided the collaterals are free from tumor invasion.

In the series reported until now, division of the GDA during PD in patients with CAS did not always result in ischemic

Fig. 1. A. On superior mesenteric arteriography, the common hepatic artery and splenic artery were visualized serially via the gastroduodenal artery. The arrow shows the root of the celiac axis. B. Sagittal reformatted CT image reveals severe stenosis (arrow) of the celiac axis.

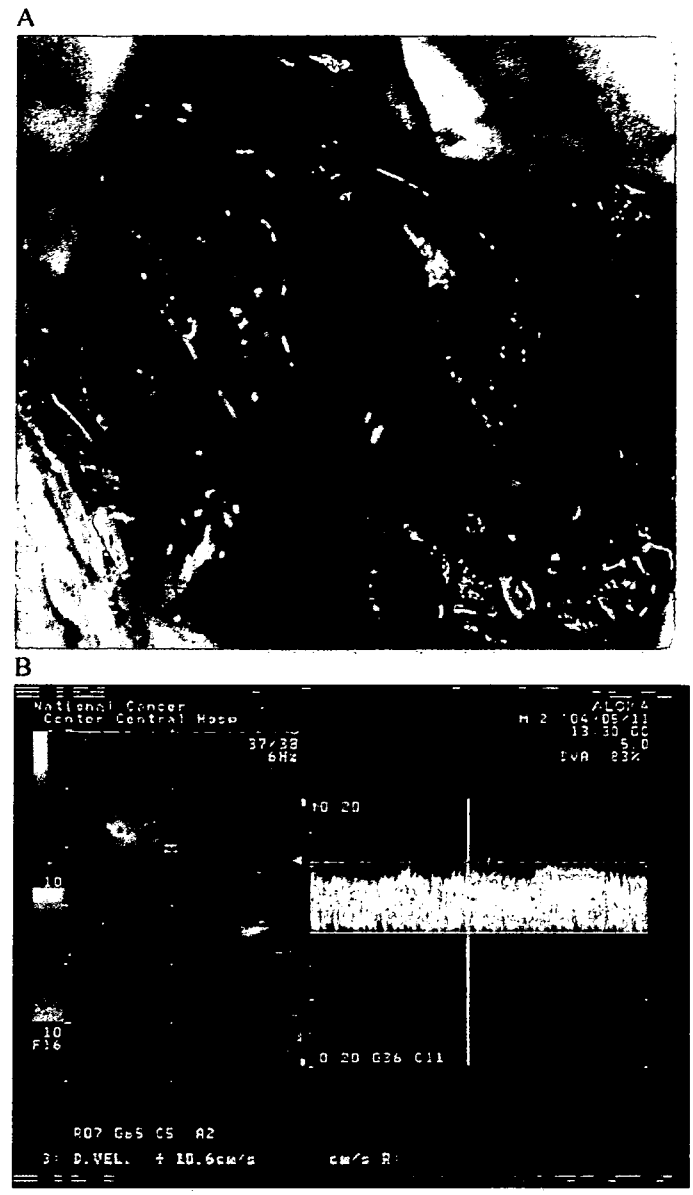

Fig. 2. A. The median arcuate ligament (arrow) masking the root of the celiac axis. B. After clamping of the gastroduodenal artery, intraoperative Doppler ultrasonography revealed an apparent decrease in the intrahepatic arterial flow.

complications of the upper abdominal organs. Both Trede [9] and Berney et al. [10] reported that only 13%–17% of patients with CAS required arterial reconstruction during PD attributed to the abundant collateral anastomosis between the CA tributaries and SMA tributaries other than the pancreatic head arcade. Among 94 Korean patients with CAS, collateral pathways, such as from the dorsal pancreatic artery or replaced right hepatic artery, existed in about 80% of the patients [12]. With these collaterals, hepatic arterial flow can be maintained even after division of the GDA, as in our case 3. However, in patients with malignant tumors, preservation of these collaterals during PD is often impossible, or it may be undesirable on account of the need to ensure surgical curability, and arterial restoration may become imperative.

We believe that intraoperative Doppler US is highly useful for informing the decision for or against arterial reconstruction, as shown in cases 1 and 2. The usefulness of intraoperative Doppler US has been demonstrated during liver transplantation [13], and this practical and convenient modality has now become indispensable for the confirmation of arterial flow during hepatobiliary-pancreatic surgery. We propose that a final decision on arterial reconstruction before the division of GDA be made using intraoperative Doppler US.

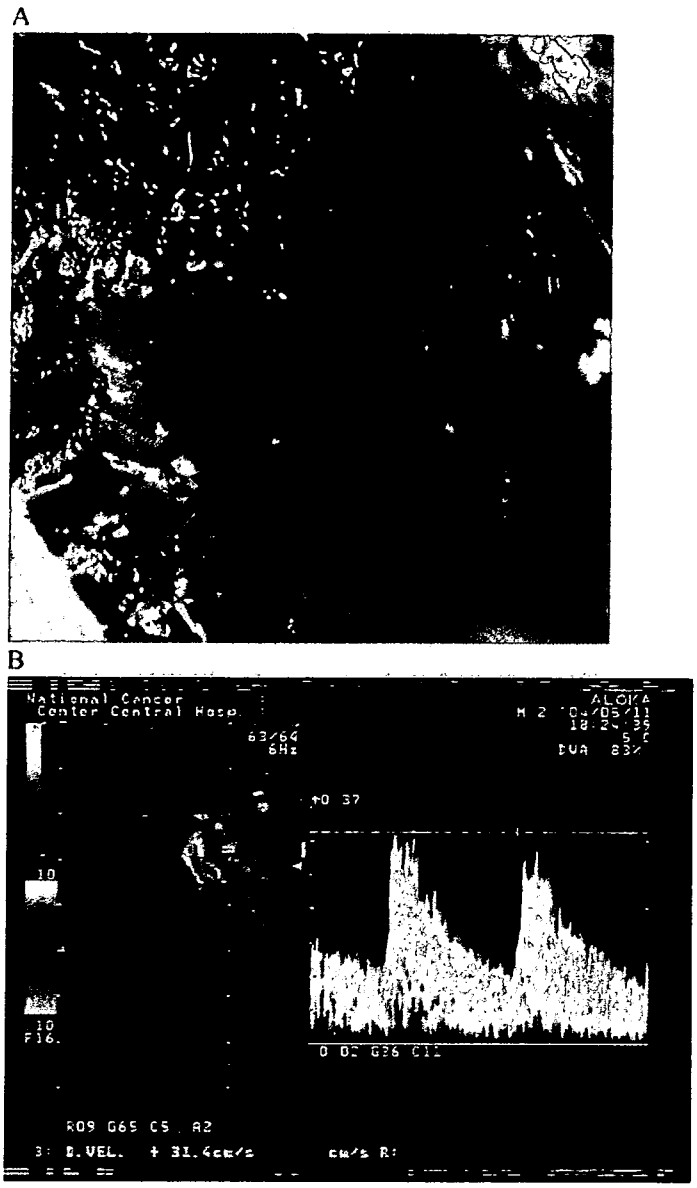

Fig. 3. A. The root of celiac axis (arrow) is exposed. B. Doppler ultrasonography shows a dramatic increase in the intrahepatic arterial signal.

The etiology of CAS can be divided into three categories;(1) extrinsic stenosis from compression by the MAL or the celiac ganglion. (2) intrinsic stenosis from atherosclerosis, (3) other causes, including congenital causes, tumor invasion, compression by a swollen pancreas in cases of pancreatitis, or injury during angiography [10, 14]. In a Korean report, among 400 consecutive angiographic examinations in patients with liver tumors, 7:3% showed CAS, and the etiology was determined to be extrinsic compression in 55% of patients, intrinsic stenosis in 10%, and other causes, in 35% [14]. In contrast, in Western studies, the most frequent etiology was atherosclerosis [10].

Revascularization procedures must be chosen according to the etiology of CAS. When CA stenosis is caused by extrinsic compression, division of the MAL or the fibrous celiac ganglion is a simple and effective method, as in case 1. Preoperative stenting of

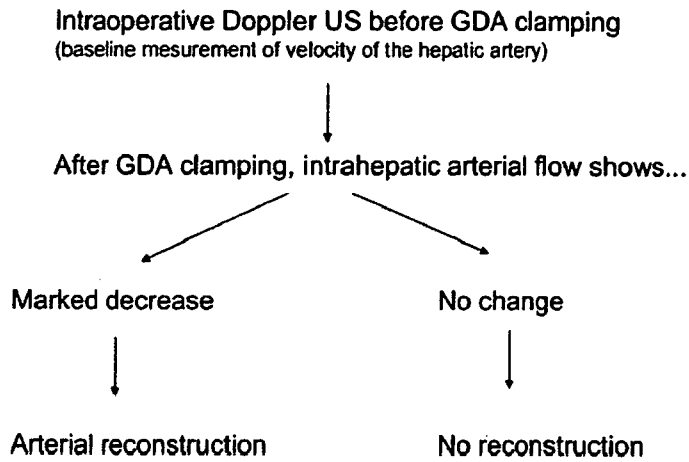

Fig. 4. Recommended steps for the decision on arterial reconstruction.

the CA, although reported to be successful in one reported case [15], was avoided by us, because of the risk of stent-crushing due to persistent external compression, as described by Sharafuddin et al. [16]. For patients with an atherosclerotic etiology, there are many reports of successful endovascular treatments [16, 17]. While the immediate success rate has been reported to be 81%–96%, the long-term success rate still remains unknown.

As for surgical reconstruction, a variety of methods have been reported, such as bypass between the aorta and the CA [4], between the splenic artery and the SMA [5], or between the aorta and the common hepatic artery, occasionally using a venous graft [2, 3]. Machado et al. reported successful reconstruction by means of anastomosis of the MCA to the GDA stump [6]. Okamoto et al. advocate a venous graft bypass between the iliac artery and the splenic artery, because the vascular anastomosis is away from the pancreatojejunostomy and the risk of exposure to pancreatic juice is minimal [7]. Thus, there is no single best procedure, and the method of arterial reconstruction used must be selected according to the surgical condition of the individual patient.

In our series, all three patients (Cases 3–5) who showed no decrease of hepatic inflow after GDA clamping developed no ischemic complication, possibly because there were enough hepatopetal collateral arteries. We therefore suppose that sustained hepatic flow after the GDA clamping indicates no need for arterial reconstruction if collaterals can be preserved. Nevertheless we believe that any patient who demonstrates a decrease in hepatic arterial flow after GDA clamping has the possibility of suffering from ischemic complications. We recommend arterial reconstruction when a moderate or severe decrease in hepatic arterial inflow is observed with Doppler US (Fig. 4). But this is a small number of patients. To establish definitive criteria for hepatic arterial reconstruction during PD for patients with CAS, a large number of patients should be studied based on the precise evaluation of the velocity of hepatic arterial inflow using Doppler US.

In conclusion, we performed PD in seven patients with CAS and encountered ischemic complications in two who underwent no arterial reconstruction. Another two patients underwent arterial reconstruction based because we observed a decrease in intrahepatic arterial flow, and neither of them developed ischemic complications. Three other patients who showed no decrease intrahepatic arterial flow on Doppler US after clamping of the GDA had an uncomplicated postopuative course. We therefore

consider that hepatic arterial reconstruction is necessary during PD in patients with CAS when intraoperative Doppler US shows a significant decrease in intrahepatic arterial signal after clamping of the GDA.

References

1. Kwon JW, Chung JW, Song SY, et al. Transcatheter arterial chemoembolization for hepatocellular carcinomas in patients with celiac axis occlusion. J. Vase. Interv. Radiol. 2002;13:689–694
2. Miyata M, Takao T, Okuda A, et al. Pancreatoduodenectomy for periampullary cancer associated with celiac occlusion: a case report. Surgery 1988;103:261–263
3. Manabe T, Baba N, Setoyama H, et al. Venous bypass grafting for celiac occlusion in radical pancreaticoduodenectomy. Pancreas 1991; 6:368–371
4. Takach TJ, Levesay JJ, Reul GJ Jr., et al. Celiac compression syndrome: tailored therapy based on intraoperative findings J. Am. Coll. Surg. 1996;183:606–610
5. Thompson NW, Eckhauser FE, Talpos G, et al. Pancreaticoduodenectomy and celiac occlusive disease. Ann. Surg. 1981;193:399–406
6. Machado MC, Penteado S, Montagnini AL, et al. An alternative technique in the treatment of celiac axis stenosis diagnosed during pancreaticoduodenectomy. HPB Surg. 1998;10:371–373
7. Okamoto H, Suminaga Y, Toyama N, et al. Autogenous vein graft from iliac artery to splenic artery for celiac occlusion in pancreaticoduodenectomy. J. Hepatobiliary Pancreat. Surg. 2003;10:109–112
8. Kurosaki I, Hatakeyama K, Nihei KE, et al. Celiac axis stenosis in pancreaticoduodenectomy. J. Hepatobiliary Pancreat. Surg. 2004; 11:119–124
9. Trede M. The surgical treatment of pancreatic carcinoma. Surgery 1985;97:28–35
10. Berney T, Pretre R, Chassot G, et al. The role of revascularization in celiac occlusion and pancreatoduodenectomy. Am. J. Surg. 1998; 176:352–356
11. Pfeiffenberger J, Adam U, Drognitz O, et al. Celiac axis stenosis in pancreatic head resection for chronic pancreatitis. Langenbecks Arch. Surg. 2002;387:210–215
12. Song SY, Chung JW, Kwon JW, et al. Collateral pathways in patients with celiac axis stenosis: angiographic-spiral CT correlation. Radiographics 2002;22:881–893
13. Sakamoto Y, Harihara Y, Nakatsuka T, et al. Rescue of liver grafts from hepatic artery occlusion in living-related liver transplantation. Br. J. Surg. 1999;86:886–889
14. Park CM, Chung JW, Kim HB, et al. Celiac axis stenosis: incidence and etiologies in asymptomatic individuals. Korean J. Radiol. 2001;2:8–13
15. Hasegawa K, Imamura H, Akahane M, et al. Endovascular stenting for celiac axis stenosis before pancreaticoduodenectomy. Surgery 2003;133:440–442
16. Sharafuddin MJ, Olson CH, Sun S, et al. Endovascular treatment of celiac and mesenteric arteries stenoses: applications and results. J. Vasc. Surg. 2003;38:692–698
17. van Wanroij JL, van Petersen AS, Huisman AB, et al. Endovascular treatment of chronic splanchnic syndrome. Eur. J. Vasc. Endovasc. Surg. 2004;28:193–200

complications of cyberknife have been reported (Table 1). Our patient developed a colonic apple-core lesion secondary to inflammatory changes after the cyberknife intervention. The presence of such a lesion proven to be nonmalignant has not been reported previously. It can be predicted that as more patients with unresectable abdominal malignancies, such as pancreatic carcinoma, are treated with cyberknife technology, more intra-abdominal radiation-induced complications will be recognized.

Although colonic apple-core lesions seen on radiology are considered to represent carcinoma unless proven otherwise, it is important to recognize that it may be caused by radiosurgery consequences. Although the future of cyberknife is promising, its complications should be considered when trying to minimize injury to the adjacent tissues.

ACKNOWLEDGMENTS

The authors thank Russel Saxton, MD, Mt Sinai, for his assistance with interpretations of the radiology films, and Tony Benito, photographer, Mt Sinai, for refining the quality of the images.

Roxane Scemla*
S. Mubashir Shah, MD†
Michael Schwartz, MD‡
Jamie S. Barkin, MD, MACG, FACP§
*Department of Gastroenterology
Ross University, School of Medicine/
Mt Sinai Medical Center
†Department of Gastroenterology
Mt Sinai Medical Center
‡Department of Oncology
Mt Sinai Medical Center
and §Division of Gastroenterology
University of Miami, School of Medicine/
Mt Sinai Medical Center Miami, Florida

REFERENCES

1. Chua YJ, Cunningham D. Adjuvant treatment for resectable pancreatic cancer. *J Clin Oncol*. 2005;23:4532–4537.
2. Randall B. Pancreatic cancer. *J Gastroenterol*. 2004;50:545–555.
3. Cheng Y, Gabor J, Zbigniew P. Measurements of the relative output factors for cyber knife collimators. *Neurosurgery*. 2004;54:157–162.
4. Cheng Y, Main W, Taylor D, et al. An anthropomorphic phantom study of the accuracy of cyberknife spinal radiosurgery. *Neurosurgery*. 2004;55:1138–1145.
5. Friedman W. Linear accelerator–based radiosurgery for vestibular schwannoma. *Neurosurg Focus*. 2003;14:2.
6. Pollock B. Stereotactic radiosurgery for intracranial meningiomas: indications and results. *Neurosurg Focus*. 2003;14:2.
7. Chua D, Shan J, Kwong P, et al. Linear accelerator–based stereotactic radiosurgery for locally persistent and recurrent nasopharyngeal carcinoma: efficacy and complications. *Int J Radiat Oncol Biol Phys*. 2003;56:177–183.
8. Lee S, Choi E, Park H, et al. Stereotactic body frame based on radiosurgery on consecutive for primary or metastatic tumors on lung. *Strahlenther Onkol*. 2003;40:309–315.
9. Benzyl D, Saboori M, Mogilner A, et al. Safety and efficacy of stereotactic radiosurgery for tumors of the spine. *J Neurosurg*. 2004;101:413–418.
10. Pham C, Chang S, Jones P, et al. Preliminary visual field preservation after stage cyberknife radiosurgery for perioptic lesions. *Neurosurgery*. 2004;54:799–812.

Imaging Features of Large Intraductal Papillary Mucinous Carcinoma of the Pancreatic Tail

Abbreviations: IPMT, intraductal papillary mucinous tumor, MCT, mucinous cystic tumor, US, ultrasound, CT, computed tomography, MPD, main pancreatic duct, MRCP, magnetic resonance cholangiopancreatography

To the Editor:

Pancreatic mucin-producing tumors, such as intraductal papillary mucinous tumor (IPMT) and mucinous cystic tumor (MCT),[1,2] are good candidates for surgical resection because of their low-grade malignant potential. It is sometimes difficult to differentiate between IPMT and MCT on imaging studies because the 2 entities sometimes show similar cystic findings. We encountered 2 patients with a large malignant IPMT in the pancreatic tail, which showed common impressive imaging features and similar pathological findings.

CASE 1

A 68-year-old man with no symptom was admitted to our department with the diagnosis of a pancreatic tumor. Ultrasound (US) showed a large, pear-shaped, low-echoic lesion between the stomach and spleen. In the cystic lesion, numerous echogenic lines with spontaneous wavelike movements were seen (Fig. 1A). Dynamic computed tomography (CT) scan demonstrated a large, pear-shaped cystic tumor, 13 cm in diameter, with multilocular margins on its caudal part in the tail of the pancreas. The edge of the pancreatic parenchyma was deformed into a beak shape ("beak sign"),[3] which represented a firm continuity of the tumor with the main pancreatic duct (MPD) (Fig. 1B). Magnetic resonance cholangiopancreatography (MRCP) demonstrated a very high-intensity mass with numerous streaks along the major axis, referred hereafter as a "brushing sign," which was thought to represent the mucinous component of the tumor. Several cystic dilatations of the branch duct in the head and body of the pancreas were also found (Fig. 1C). The preoperative diagnosis was multicentric IPMTs, one of which exhibited a tremendous growth in the tail of the pancreas. Distal pancreatectomy was performed. The histological finding was intraductal papillary mucinous carcinoma with invasion slightly beyond the duct wall, that is, with minimal invasion [4,5] (Fig. 1D). In the mucus pool of the markedly dilated MPD, the tumor cells were peeled off and floating with their corpses.

CASE 2

A 61-year-old woman who had repeated pancreatitis was referred to our department for the treatment of a large cystic tumor in the tail of the pancreas. On US, a large low-echoic lesion was visualized in a spindle form, and numerous echogenic streaming patterns were seen therein. A CT scan revealed a large low-attenuating tumor, 13 × 5 cm in size, in the tail of the pancreas. A beak sign was also found in the tail of the pancreas. Several mural nodules suggested the presence of malignant component. On MRCP, the brushing signs were also observed within the cystic tumor. Distal pancreatectomy was performed. The pathological diagnosis was intraductal papillary mucinous carcinoma with minimal invasion.

A differential diagnosis between IPMT and MCT is sometimes difficult. Both tumors can contain mucinous components and have malignant potentials, especially when the tumor has mural nodules or solid components.[6] IPMT is located in the pancreatic head in 60% of patients and sometimes exhibits intraductal spread[7] or multicentric occurrence along MPD[8] and is continuous with the MPD.[6] On the other hand, MCT arises from the pancreatic tail in

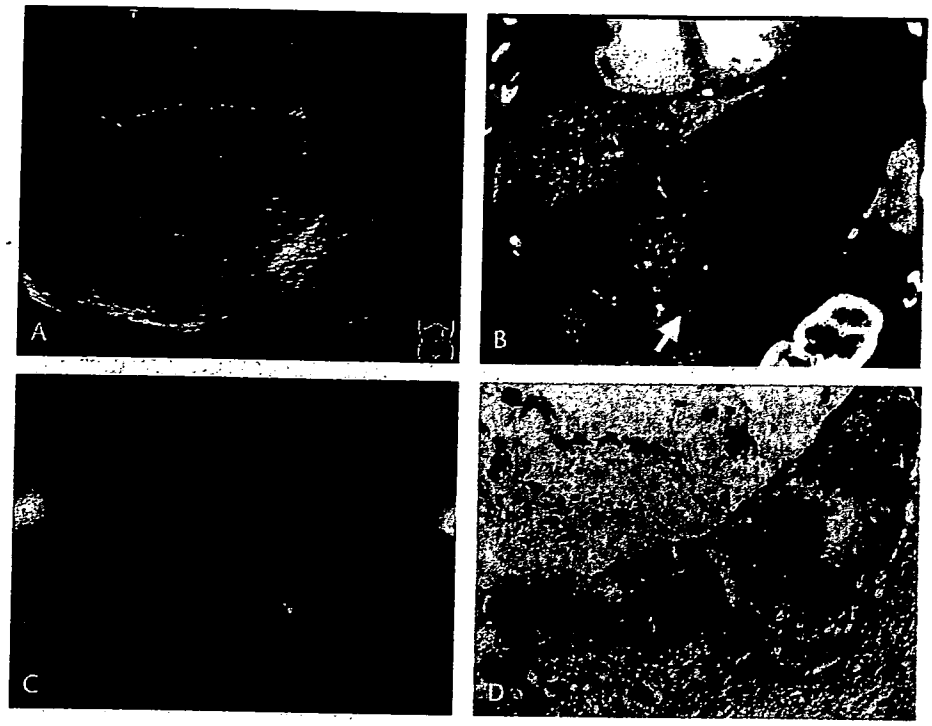

FIGURE 1. A, Abdominal US shows numerous streaming lines that spontaneously move in a wavelike manner inside the cystic tumor in a sagittal direction. B, Coronal reformatted CT scan reveals "a beak sign" (arrow) between the cystic tumor of the pancreatic tail and the MPD. C, MRCP shows a very high-intensity mass with "a brushing sign" inside the tumor of the pancreatic tail. Several cystic lesions are also present in the head and body of the pancreas. D, The irregular papillary projections are composed of tall columnar cells with nuclear atypia, and part of the tumor has collapsed, forming the streaked structures in the mucous pool with epithelial corpses (upper left, hematoxylin-eosin, magnification ×200).

70% to 90% of patients,[6,9] with a higher prevalence in women,[1,2] and is rarely continuous with MPD.[5] MCT can be pathologically characterized as ovarian-type stroma.[2] In the present cases, multicentric occurrence in CASE 1 and mural nodule in CASE 2 also suggested IPMT rather than MCT.

The impressive common imaging features of the 2 megacystic lesions were (1) a beak sign on CT images, suggesting a pancreatic origin and the distinct continuity of the cystic part with MPD, and (2) a brushing sign on MRCP, which might express moving mucinous components with a large amount of peeled epithelium and their corpses, floating inside the tumor. In the diagnosis of megacystic tumor in the tail of the pancreas, the beak sign and brushing sign might be helpful to differentiate IPMT from MCT.

Yu Takahashi, MD*
Yoshihiro Sakamoto, MD*
Kazuaki Shimada, MD*
Tsuyoshi Sano, MD*
Tomoo Kosuge, MD*
Hiroaki Onaya, MD†
Yasunori Mizuguchi, MD†
Nobuyoshi Hiraoka, MD‡
*Hepatobiliary and Pancreatic Surgery Division
†Diagnostic Radiology Division; and
‡Pathology Division
National Cancer Center Research Institute
Tokyo, Japan

REFERENCES

1. Klöppel G, Solcia E, Longnecker DS, et al. Histological typing of tumors of the exocrine pancreas. In: *WHO International Histological Classification of Tumors*, 2nd ed. New York: Springer-Verlag; 1996.
2. Solica E, Capella C, Klöppel G. Tumors of the pancreas. *Atlas of Tumor Pathology, 3rd series, Fascicle 20*. Washington, DC: Armed Forces Institute of Pathology; 1997.
3. Nishino M, Hayakawa K, Minami M, et al. Primary retroperitoneal neoplasms: CT and MR imaging findings with anatomic and pathologic diagnostic clues. *Radiographics*. 2003;23:45–57.
4. Fukushima N, Mukai K, Kanai Y, et al. Intraductal papillary tumors and mucinous cystic tumors of the pancreas: clinicopathologic study of 38 cases. *Hum Pathol*. 1997;28: 1010–1017.
5. Zamboni G, Scarpa A, Bogina G, et al. Mucinous cystic tumors of the pancreas. Clinicopathological features, prognosis, and relationship to other mucinous cystic tumors. *Am J Surg Pathol*. 1999;23:410–422.
6. Sugiyama M, Atomi Y. Intraductal papillary mucinous tumors of the pancreas. Imaging studies and treatment strategies. *Ann Surg*. 1998;228:685–691.
7. Fukushima N, Mukai K. Differential diagnosis between intraductal papillary-mucinous tumors and mucinous cystic tumors of the pancreas. *Int J Surg Pathol*. 2000;8: 271–278.
8. Obara T, Saitoh Y, Maguchi H, et al. Multicentric development of pancreatic intraductal carcinoma through atypical papillary hyperplasia. *Hum Pathol*. 1992;23:82–85.
9. Sarr MG, Carpenter HA, Prabhakar LP, et al. Clinical and pathologic correlation of 84 mucinous cystic neoplasms of the pancreas. Can one reliably differentiate benign from malignant (or premalignant) neoplasms? *Ann Surg*. 2000;231:205–212.